Journal of Materials Chemistry A

Accepted Manuscript

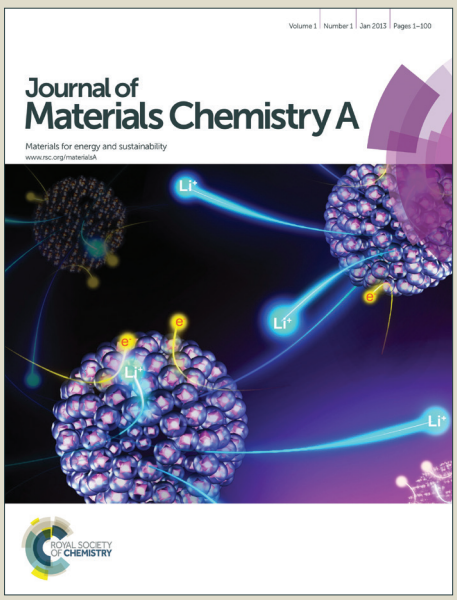

ROYAL SOCIETY OF CHEMISTRY

www.rsc.org/materialsA

Accurate surface control of core-shell structured $LiMn_{0.5}Fe_{0.5}PO_4$@C for improved battery performance

Zi-Xiang Chi [a], Wei Zhang [a], Xu-Sheng Wang [b], Fu-Quan Chen [b], Ji-Tao Chen [b], An-Min Cao* [a], Li-Jun Wan* [a]
E-mail address: anmin_cao@iccas.ac.cn, wanlijun@iccas.ac.cn

[a] *Key Laboratory of Molecular Nanostructure and Nanotechnology and Beijing National Laboratory for Molecular Sciences, Institute of Chemistry, Chinese Academy of Sciences (CAS), Beijing 100190, PR China*

[b] *College of Chemistry and Molecular Engineering, Peking University, Beijing 100871, PR China*

Abstract

Manganese-based mixed polyanion cathodes known as $LiMn_{1-x}Fe_xPO_4$ can show much higher energy density as compared to the well-commercialized product of lithium iron phosphate. However, their much lower electronic conductivity has long plagued their further application. Here, by means of a facile solution-based synthesis route, we are able to introduce a uniform and conformal carbon coating layer onto the $LiMn_{1-x}Fe_xPO_4$ nanoparticles. The versatility in the synthesis control endows us the capability of controlling the shell thickness with one nanometer accuracy, offering an effective way to optimize the battery performance through a systematic shell control. Detailed investigation reveals that the carbon nanoshells not only act as a good electronic conducting media, but also contribute to inhibit the metal (Mn and Fe) dissolutions and reduce the exothermic heat released during cycling. The core-shell structured cathode materials show promising potential for their application in lithium ion batteries as revealed by their high charge/discharge capacity, remarkable thermal stability, and excellent cyclability.

Key word

Core-shell structure, lithium ion batteries, carbon coating, thickness control, cathode materials

Introduction

Polyanion-type transition metal phosphates $LMPO_4$ (M=Fe, Mn, Ni or Co) have been widely recognized as a kind of potential cathode materials for rechargeable LIBs owing to their excellent thermal stability, environmental benignity, and low cost. [1-4] Among them, $LiFePO_4$ (LFP) is the most successfully applied material which has already been commercialized and put into

production on large scale. Nevertheless, due to the 1D Li^+ transport in the olivine crystal structure, the intrinsic low electronic conductivity and low ion diffusion rate of Li^+ is still the main obstacle which limits its industrial applications. [5, 6] Compared to LFP, $LiMnPO_4$ (LMP) has attracted much recent study interest for the higher Li^+ intercalation potential at 4.1V vs Li^+/Li than that for $LiFePO_4$ (3.4 V vs Li^+/Li), [7] which provides about 20% higher energy density than LFP. [8, 9] However, the electrical conductivity of LMP is even lower than LFP by five orders of magnitudes, making it unable to achieve high enough capacity at high rates. [7, 10] Doping LMP with a portion of Fe, namely forming a $LiMn_{1-x}Fe_xPO_4$ ($0<x<1$), turns out to be a realistic way to combine the virtues of both LFP and LMP together, which not only provides the higher operate voltage and energy density, [11] but also can partially alleviate its low electronic conductivity. [12]

The introduction of a conducting matrix, usually carbon, has been widely-accepted as an effective way to improve the electrochemical performance of polyanion-type cathode materials. [13, 14] As far as the electronic conductivity is concerned, core-shell structured cathode materials with a uniform and conformal surface layer are reasonably desirable since full carbon coverage can ensure a better contact between different particles with no dead zones and further build conductive networks, which can effectively reduce the polarization and improve the rate-capability during the charge/discharge process. [13] However, the transportation of lithium ion is also needed to be considered since the existence of a surface layer on the cathode material will be an additional barrier, which will affect the diffusion of lithium ion transport and then determines the interfacial charge-transfer resistance between electrode and electrolyte. [15] Therefore, an optimization on the core-shell structure is also expected so that a balance between the electronic conductivity and lithium ion diffusion can be achieved. Equally important, the synthesis protocol should be simple and economic, showing the capability of scaling up for the production of large quantity of powders with satisfied quality on the surface control. In this way, a critical condition of the coatings layer could be determined and an optimal battery performance could be delivered.

Recently the polymerization of resorcinol-formaldehyde (RF) has aroused people's attention for its potential in surface coating.[16, 17] It is proposed that the formation of RF nanospheres will go through a sol-gel process similar to what happened during the formation of colloidal silica.[18, 19] Inspired by the fact that such a sol-gel process has been highly effective to introduce a surface coating layer of silica, researchers then start to discuss the possibility of creating RF coatings and

also carbon coatings after a following graphitization process. [20-22] During our pursuit for an ideal coating process for polyanion-type cathode materials, the RF polymer turns out to be a perfect choice. First, the process is economically favorable with the use of cheap industrial raw materials in an aqueous phase-dominant solution. Second, the weak alkali condition during the RF formation would not do harm to the core materials of cathode materials, which are known to be susceptible to acidic conditions.

Herein, we successfully applied the in-situ resorcinol-formaldehyde (RF) polymerization process to the surface carbon coating of cathode materials. Typical core-shell structures as $LiMn_{0.5}Fe_{0.5}PO_4$@carbon (LMFP@C) are created with uniform carbon nanoshells on the surface. Interestingly, the shell thickness can be accurately controlled nanometer-by-nanometer thanks to the versatility in the synthesis control. Accordingly a systematic evaluation on the coating effects becomes possible due to this synthesis advantage. It is found that the battery performance of the core-shell structured cathode materials is highly related to the surface shell and a 3 nm carbon coating on LMFP provides the best result. Further investigation shows that the carbon nanoshell not only contributes as an electronic conductor, but also can alleviate the Fe dissolution and reduce the exothermic heat released during cycling. The optimized LMFP@C cathode material shows high charge/discharge capacity, remarkable thermal stability, and excellent cyclability, which promised good potential for their application in lithium ion battery.

Results and discussion

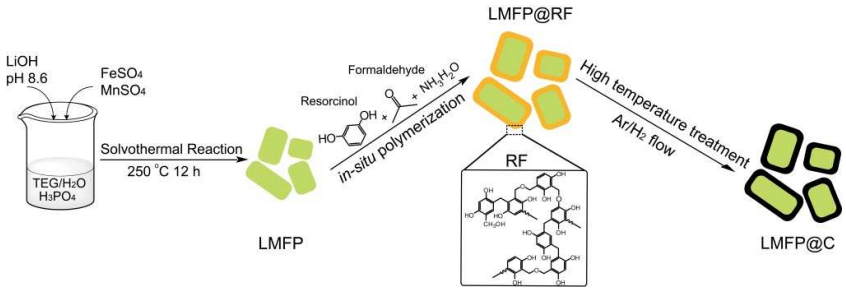

Scheme 1. Schematic illustration of the synthesis of LMFP@C composites and the coating mechanism of RF polymerization.

The formation of LMFP@C composites is schematically illustrated in Scheme 1. Firstly LMFP powder is prepared and then it is used as seeds for surface coating. Resorcinol and formaldehyde will polymerize on the surface of LMFP to form a thin layer of RF resin, forming a core shell structure with LMFP as the core and RF resin as the shell (denoted as LMPF@RF). Finally a high

temperature treatment under a reductive atmosphere can transfer the RF resin into conductive carbon and LMFP@C forms as the cathode materials for further characterizations.

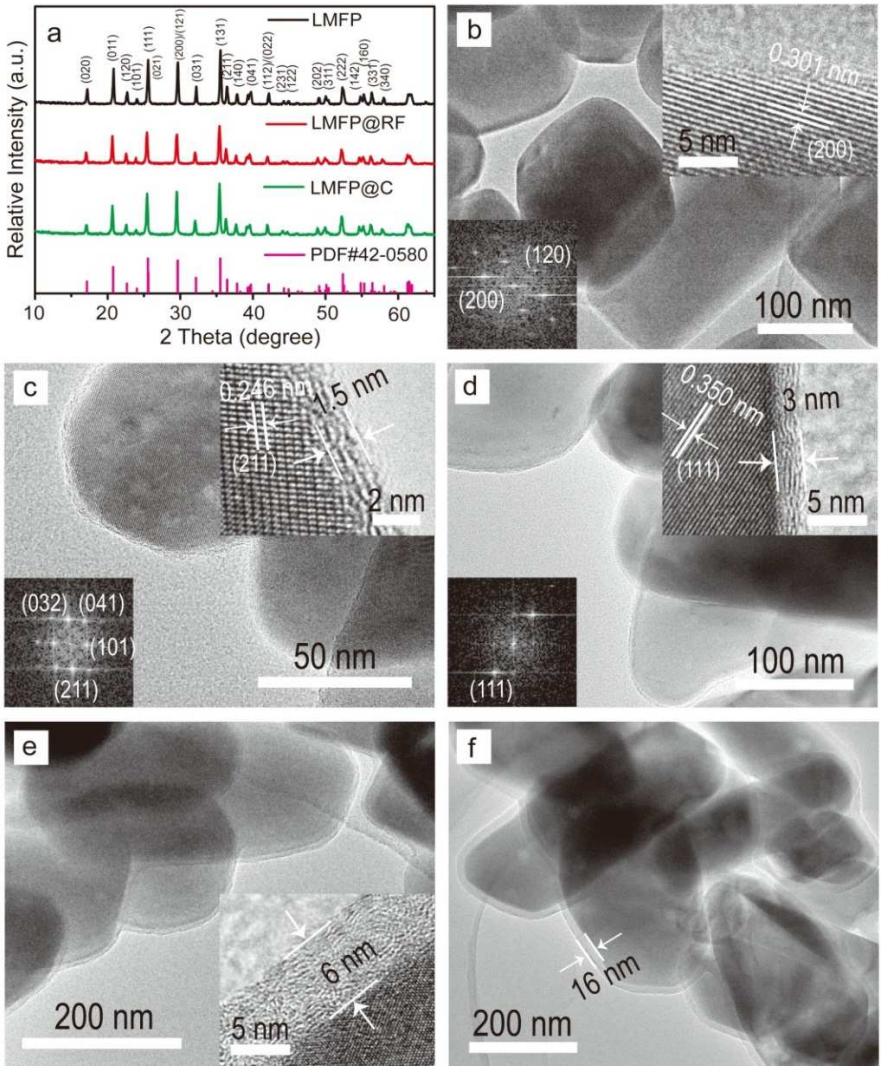

Figure 1. (a) XRD patterns of the hydrothermally synthesized LMFP, LMFP@RF2, and LMFP@C2, respectively. (b-f) TEM images of LMFP (b), LMFP@C1 (1.5 nm coating) (c), LMFP@C2 (3 nm coating) (d), LMFP@C3 (6 nm coating) (e) and LMFP@C4 (16 nm coating) (f).

The core material as LMFP is synthesized by means of a solvothermal route (Seeing supporting information for details). The X-ray diffraction (XRD) characterization on the newly-prepared sample confirms the formation of highly crystalline LMFP as shown in Fig. 1a (JCPDS no. 42-0580). The sample's morphology can be obtained by using transmission electron microscopy (TEM) and Fig. 1b showed a representative image. The particles are rod-like in shape and have a size ranging from 200 nm to 500 nm (SEM image shown in Fig. S3a). The high resolution TEM

(HRTEM) characterization on a randomly-selected particle reveals that it is highly crystalline with a free surface borderline (inset in Fig. 1b). After the above-mentioned coating treatments, namely the RF polymerization and its following graphitization, the LMFP particle shows observable change on its morphology, specifically its surface structure. As shown in Fig. 1c, a very thin layer emerges on each LFMP particle when a very low concentration of resorcinol monomer (6.055 mM) is used during the polymerization step. A close observation by HRTEM reveals the existence of a surface shell around the particle. The thickness is around 1.5 nm (Inset in Fig 1b) and it distributes evenly on the LFMP core, forming a typical core-shell structure (denoted as LMFP@C1).

The core-shell configuration can be further manifested when a thicker shell is created on the surface. In our synthesis, we found that the coating layer can be well regulated by controlling the concentrations of the reactant or varying the polymerization time. Not surprisingly, either an increase in the resorcinol concentration or a smaller amount of LMFP seeds will lead to a thicker shell. For example, when we decrease the concentration of LMFP seeds from 183.65 mM to 113.02 mM while keep the concentration of resorcinol unchanged, a thicker surface layer is acquired as shown in Fig. 1d (sample denoted as LFMP@C2). Its HRTEM image (inset in Fig. 1d) shows that the thickness is doubled and reaches 3 nm. There exist observable lattice fringes of graphite carbon in the surface coating layer as a result of the graphitization process. The surface thickness can be further doubled when 70.63 mM LMFP seeds and 10.93 mM resorcinol are used as shown in Fig. 1e (sample denoted as LFMP@C3). Similarly, by modulating the reactant concentrations, we managed to control the carbon layer at different levels. As a matter of fact, our synthesis efforts reveal that it is possible to control the surface coating layer with one nanometer accuracy. Fig. S1 shows representative samples we prepared with their thicknesses at 2, 5, 8 and 10 nm, respectively. Further concentration control can produce even thicker nanoshells as shown in Fig. 1f, which identifies the formation of a 16 nm nanoshell around LMFP particles (sample denoted as LMFP@C4).

The above controlled nanoshells were fulfilled under the fixed reaction time of 20 h for RF polymerization onto LMFP particles. Benefiting from the versatility of the analogous sol-gel formation of RF resin, [17, 23] it is also possible to modulate the coating layer by simply varying the polymerization time. For instance, if the RF polymerization was terminated after 1.5 h, 3 h, 6 h and 12 h respectively in the synthesis of LMFP@C4, carbon shells of 2.5, 4, 7 and 12 nm were

obtained after graphitization as shown in Fig. S2. It is worthwhile to note that no obvious changes on the XRD patterns between LMFP@RF and LMFP@C could be identified (Fig. 1a). Meanwhile, their SEM (Fig. S3) images showed that these two samples had the same shapes. Elemental analysis (Table S1) by means of inductively coupled plasma-atomic emission spectroscopy (ICP-AES) confirmed that the Mn/Fe ratio remained almost constant around 1. It was therefore concluded that the graphitization process did not affect the crystal structure of LMFP in a discernible way.

To further locate the distribution of carbon in the sample, we carried out detailed elemental analysis on different samples. Fig. 2 shows the elemental mappings of a representative sample of LMFP@C3 by using the technique of scanning TEM (STEM). The image mode of STEM shows the morphology of the selected particles and it is also easy for us to see the surface coating layer (Fig. 2a). As expected, a homogeneous distribution of both Fe and Mn can be detected as shown in Fig. 2b and 2c, confirming the formation of LMFP as the core materials. The atomic ratio between Mn and Fe is measured to be 5.52:5.44 (Fig. 2e), which is in good agreement with the theoretical value. As for the carbon element, it distributes all across each LMFP particle, which is the typical characteristic of a core-shell structures. Further element analysis did not find any independent carbon nanoparticle. It is therefore concluded that all the carbon species exist around the LMFP particle as a coating layer while no phase separation happens between LMFP and carbon.

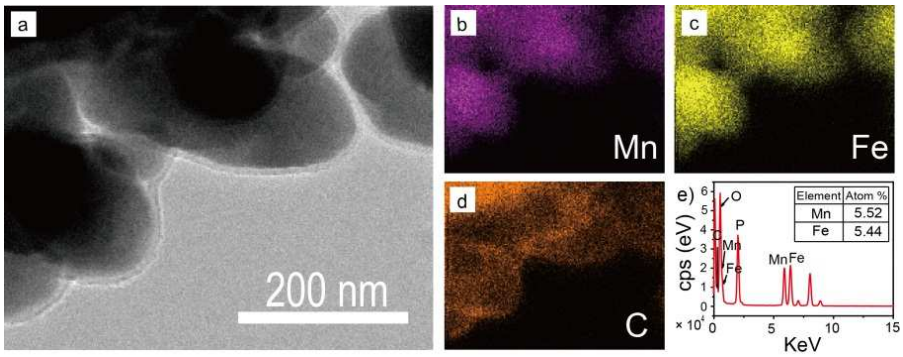

Figure 2. Representative elemental mappings on LMFP@C3 sample.

The surface carbon is introduced by a graphitization process from the original RF polymer. For the above-mentioned LMFP@C samples, their corresponding precursors as LMFP@RF have also been examined to study the effect of the high temperature treatment. As shown in Fig. S4, these LMFP@RF precursors exhibit almost the same morphology as their graphitized counterparts.

They have obvious core-shell structures but with a relatively thicker coating layer on the surface. The RF shells are about 2.4, 4.2, 8.3 and 20 nm in thickness, thicker than their graphitized counterparts in LMFP@C1-4, which is reasonable considering that the high temperature graphitization process will cause mass loss and therefore shrink the surface layer. Meanwhile, Fourier-Transfer Infrared (FT-IR) and Raman spectroscopy were performed to track the surface change during the whole synthesis. Fig. 3a is IR patterns of LMFP, LMFP@C2, LMFP@RF2 and RF. Typically, the O-H stretching vibrations between 3600 and 3100 cm^{-1}, [24] the C=C stretching vibration in the aromatic rings at 1613.17 and 1451.64 cm^{-1}, [25] and the phenolic C-O-H bending and stretching vibration at 1391.81 and 1292.47 cm^{-1} [26, 27] are fingerprint ones of RF resin, confirming the existence of RF in LMFP@RF. These peaks disappear in the spectra of LMFP@C2 due to the high temperature treatment. Raman spectrum of the LMFP@C2 confirms the emergence of carbon as shown in Fig. 3b. The characteristic peaks at 1582.96 cm^{-1} and 1339.61 cm^{-1} are the Raman fingerprints for the G and D band [28, 29] of carbon, respectively. After the high temperature treatment, the RF layer is successfully transferred into a conductive carbon layer, which is highly wanted for the application of LMFP sample. The conductivity of LMFP@C2 is measured to be 6.54×10^{-2} S/cm (shown in Table S2), revealing an obvious contribution of carbon considering the fact that the LMFP was well known of its extremely low electron conductivity (lower than $LiFePO_4$,which is $10^{-9} \sim 10^{-11}$ S/cm [5]).

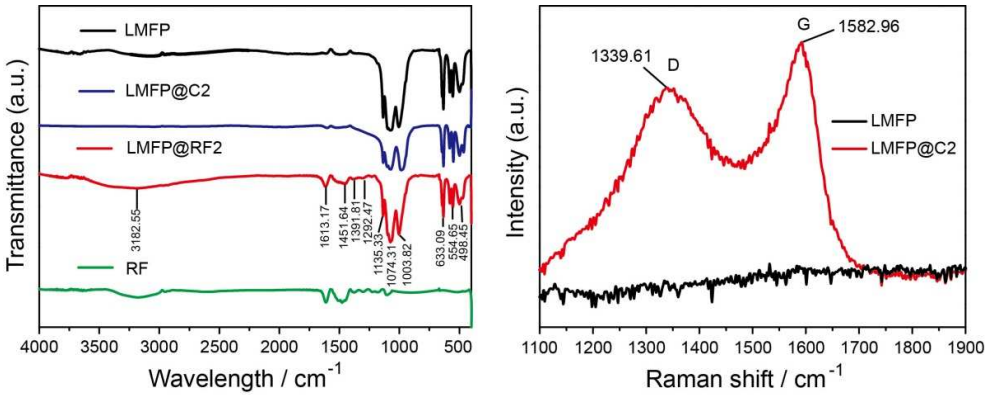

Figure 3. (a) IR spectra of LMFP, LMFP@C2, LMFP@RF2 and RF; (b) Representative Raman spectra of carbon coated LMFP@C sample with a coating thickness of 3 nm.

The accurate surface control of LMFP@C provides an ideal model system for the evaluation and optimization of its electrochemical performance. We have carried out systematical

experiments on the LMFP@C samples with their shell thicknesses controlled at one-nanometer-difference. The battery performance of a series of tested samples is found to be closely related to the shell thickness. Fig. 4a shows the charge/discharge curves of representative LMFP@C samples to have a clear idea of the shell impact. For the pristine LMFP sample with no surface carbon coating, it can only deliver a discharge capacity of 42.5 mAh g^{-1} at the low discharge current 0.1C (1C=170 mAh g^{-1}) in the first cycle, and no obvious plateaus can be observed due to the extremely poor conductivity and its arising polarization. Apparently, the coating strategy has effectively alleviated the conductivity issue. A very thin layer of carbon, 1.5 nm in thickness for LMFP@C1, can give a much higher discharge capacity of 133.9 mAh g^{-1} at 0.1C. The two distinct charge-discharge platforms at around 4.0 V and 3.5 V can be clearly observed, which represent the Mn^{3+}/Mn^{2+} and Fe^{3+}/Fe^{2+} redox equilibrium, indicating a much reduced polarization due to the existence of the surface coating layer. And the width ratio of the two plateaus is nearly equal, consistent with the molar ratio of Mn and Fe. The benefit from such a carbon coating becomes even more remarkable for a 3 nm nanoshell. For the sample of LMFP@C2, it produces an even higher discharge capacity of 155.4 mAh g^{-1} and accordingly much wider plateaus for Fe and Mn.

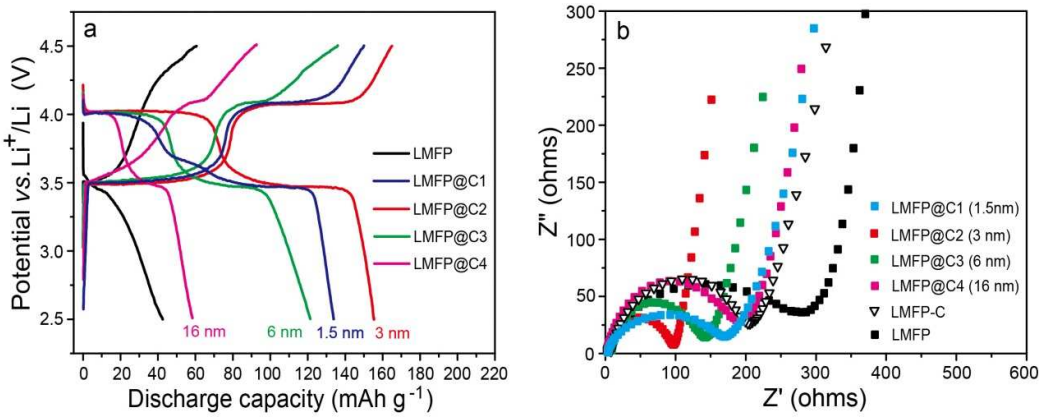

Figure 4. (a) Comparison of the first charge/discharge curves of LMFP, LMFP@C1–4 at 0.1C rate; (b) EIS spectra for LMFP, LMFP@C1–4 and LMFP-C with the frequency range of 100 kHz to100 MHz.

A thorough investigation on the coating effect reveals that further increase in shell thickness cannot benefit the battery performance. On the contrary, a gradual decline in discharge capacity is found for those samples with carbon shell thicker than 3 nm. For example, the sample of LMFP@C3 has a 6 nm carbon coating and it can deliver a discharge capacity of 124 mAh/g. For

the 16 nm carbon coating in the case of LMFP@C4 sample, a very low discharge capacity of 58.2 mA h g^{-1} is observed during its first charge/discharge cycle at 0.1C. Although a thicker carbon coating is considered to be beneficial to the electron conducting, an obvious polarization is identified in the charge curve of LMFP@C4, which is probably due to a longer diffusion distance for lithium ion.[30, 31] We use the technique of electrochemical impedance spectroscopy (EIS) to facilitate our understanding on this structure-related battery performance. Fig.4b shows the Nyquist plots for different thickness-controlled samples and LMFP@C2 has the smallest radius of the semicircle in the high-to-medium frequency range. Such a radius is known as the charge transfer and surface film resistance (R_{ct}), which is related to lithium ion interfacial transfer between the electrolyte and the active material. [32] Not surprisingly, the charge transfer and interface reaction should be much easier for the 3 nm carbon nanoshell, which also explains well its lowest polarization or its superior electrochemical performance.

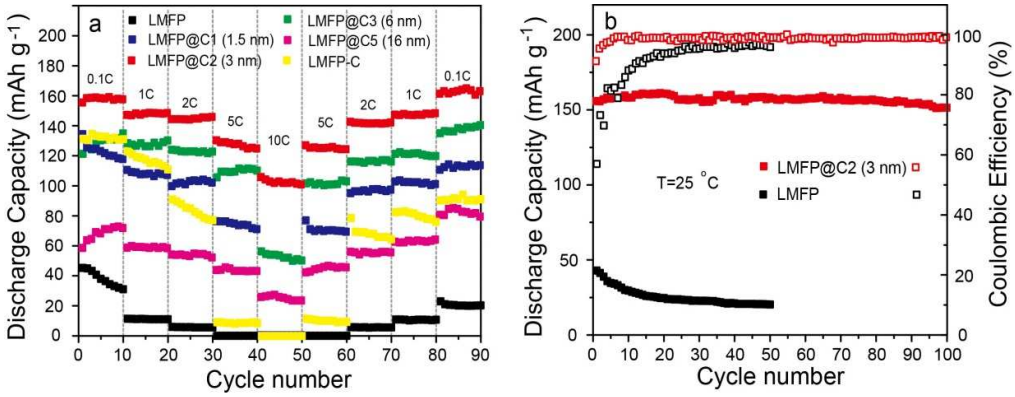

Figure 5. (a) Comparison of the rate-capability among LMFP, LMFP@C1–4 and LMFP-C; (b) comparison of the cyclability between LMFP@C2 and LMFP.

Fig. 5a shows the rate capabilities of different LMFP@C samples. Obviously, the introduction of carbon nanoshells makes these LMFP@C samples much better cathodes as long as the discharge capacity is concerned. Also, LMFP@C2 is identified as the best sample and it shows specific capacities of 155 mAh/g at 0.1 C, 147 mAh/g at 1 C, 144 mAh/g at 2 C, 129 mAh/g at 5 C and 105 mAh/g at 10C (Fig. 5b), exhibiting an extraordinary high-rate performance. For comparison, bare powder of LMFP is mixed with carbonized RF to form a sample denoted as LMFP-C, in which carbon is 2.91 % in weight, nearly the same as that of LMFP@C2. We found that the carbon additive can also be of benefit to the rate-capability of the pristine-LMFP and a discharge capacity of around 132 mAh/g is achieved. However, when it comes to higher discharge

currents, the capacity fades quickly at 1C (110 mAg/g) and 2C (77 mAh/g), and nearly no capacity can be harvested at 5 C and 10 C. Such a contrast experiment clearly highlights the significance of the core-shell configuration of LMFP@C samples. Furthermore, we also tested the cyclability of the LMFP@C2 to reveal its potential in long time usage. After 100 cycles, it still shows a discharge capacity of 151 mAh/g, about 97% of the value of the first cycle. Meanwhile, the coulombic efficiency can be constant at around 100%. In addition, the core–shell structure turns out to be pretty stable during cycling. Fig. S5 shows a TEM image of LMFP@C3 sample after being cycled for 90 times. The carbon layer is well preserved, almost the same as that before cycling. We can still observe a continuous coating on the LMFP particle. There is no detectable shedding of carbon layer and the thickness remains around 6 nm as revealed by the HRTEM image (inset in Fig. S5). We believe that such a core-shell configuration can guarantee the structure stability for the long term cycling, which is promising for its practical applications in lithium ion batteries.

At elevated temperatures, the olivine cathodes are prone to transition metal dissolution and lead to an accelerated capacity fading. [33-35] Accordingly, these polyanion-type cathodes usually show poor high-temperature performance. We found that the core-shell structure can significantly alleviate this problem as shown in Fig. 6a. For different LMFP@C samples, a very thin nanoshells as for the 1.5 nm carbon coating in LMFP@C1 still cannot sustain extended cycling at 55 ^{o}C. As shown in Fig.6a, it undergoes serious capacity fading from 161 to 3.3 mAh/g after 30 cycles. On the contrary, for thicker coating as for LMFP@C2-4, the capacity fading has been effectively alleviated. Typically, for the sample of LMFP@C4, it has a very thick coating (16 nm) and it can constantly offer a discharge capacity of 123 mAh/g with no fading at all. Meanwhile, the LMFP@C2 sample can also have a decent performance at elevated temperature. After cycling at 55 ^{o}C for 50 times, it can still deliver a capacity of 144 mAh/g, about 90 % of that for the first cycle.

Further experiments were carried out to test the structure stability of these cathode materials at high temperatures. As described in the Experimental section, the prepared cathode powders were immersed in electrolyte for extended period at 55 ^{o}C, and then the dissolved metals were analyzed by ICP-AES. As expected, the dissolutions of Mn and Fe in electrolyte were pretty serious as shown in table 1. However, a carbon coating is proved to be very effective in inhibiting the metal

dissolution. Along with the increase in carbon thickness, the metals dissolved turned less. For example, with the help of a 3 nm carbon coating, the Mn dissolution could be reduced from 632 mg/L to 326 mg/L while the Fe loss will be reduced 72.4 mg/L down to 37.2 mg/L. We also recorded the color contrast of electrolyte removed from pure LMFP and LMFP@C2 after a period of high-temperature storage, to give a visual comparison of chrominance changing, as is shown in Fig. S6. Due to the serious dissolution of Mn and Fe, the electrolyte left by LMFP shows much deeper color, which is in good agreement with the ICP measurement. When the coating thickness jumped to 16 nm for LMFP@C4, the Mn and Fe dissolution amount can be further decreased to 114.2 and 16.8 mg/L respectively.

Table 1. Metal dissolution of LMFP, LMFP@C1, LMFP@C2 and LMFP@C4 after storing for 2 weeks at 55 ^{o}C (lM $LiPF_6$ in EC: DMC: DEC=1:1:1).

	Pure LMFP (no coating)	LMFP@C1 (1.5 nm coating)	LMFP@C2 (3 nm coating)	LMFP@C4 (16 nm coating)
Mn dissolution (ppm)	632	524	326	114.2
Fe dissolution (ppm)	72.4	63.1	37.2	16.8

We also found that the surface carbon layer is very effective in reducing the exothermal heat released in the battery, which is highly favorable considering the increasingly strict safety requirement enforced by the industry of lithium ion batteries.[14, 36] Experimentally, different cathode materials are activated by charging them to a high potential of 4.5 V, and then differential scanning calorimetry (DSC) is used to record the heat released at different temperatures (seeing experimental section for details). Three different samples as pristine LFMP, LMFP@C2 and LMFP@C3 were selected for comparison. Fig. 6b presents the DSC results which are recorded in the temperature range 330-623.15 K at a heating rate of 10K min^{-1}. We actually didn't observe a big difference in the starting points of the exothermic heat flow. For example, the sample of LMFP@C3 only shows an improvement of about 20 K for the starting point. However, we found a much reduced heat release at the existence of carbon nanoshells. For the pure LMFP sample, the exothermic heat flow was detected to start from about 480 K, with total heat evolution~1000.99 J g^{-1}. While a 3 nm carbon coating can reduce the released heat to 577.93 J/g as happened to the

LMFP@C2 sample. Moreover, the total heat evolution becomes only 362.65 J/g for LMFP@C3 (6 nm coating) due to a thicker nanoshell. The reaction between the electrolyte and the cathode materials has been known as an inevitable process to release heat and cause serious safety problems. [37] By introducing a conformal nanoshell around the LMFP core, we found it can play a very active role in combating those problems as revealed by the alleviated iron dissolution and heat release. We believe that such a core-shell configuration of LMFP@C can be very promising for their practical application as cathode materials in lithium ion batteries.

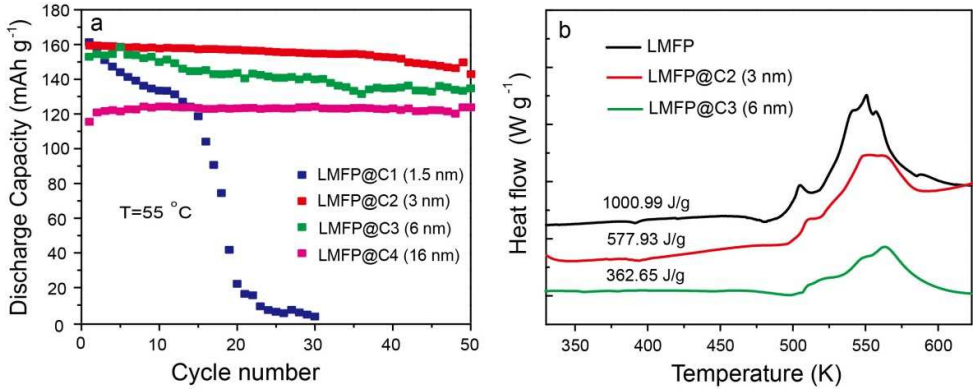

Figure 6. (a) Cyclibility of LMFP@C1-C4 measured at 55 °C; (b) DSC profiles of pure LMFP, LMFP@C2 and LMFP@C3. Charged to 4.5V.

Conclusion

In summary, core-shell structured LMFP@C has been prepared by means of the in situ polymerization of resorcinol-formaldehyde. The carbon nanoshells can be accurately controlled with its thickness being readily tuned at one nanometer level, which provides a good model system for the optimization of the battery performance of these core-shell structured cathodes. Detailed investigation identified that a 3 nm carbon nanoshell is the best coating for LMFP. The existence of carbon nanoshells not only act as a good electronic conducting media, but also contribute to inhibit the Metal dissolution and reduce the exothermic heat released during cycling. The core-shell structured cathode materials show promising potential for their application in lithium ion batteries as revealed by their high charge/discharge capacity, remarkable thermal stability, and excellent cyclability.

Acknowledgements

This work was supported by the major State Basic Research Program of China (973 program:

2013CB934000, 863 program: 2013AA030800), the National Natural Science Foundation of China (Grant no. 21373238), and the Chinese Academy of Sciences (XDA09010001).

References

[1] J. B. Goodenough, *J. Electrochem. Soc.,* **1997**, 144, 1188-1194.
[2] C. Sun, S. Rajasekhara, J. B. Goodenough, F. Zhou, *J. Am. Chem. Soc.,* **2011**, 133, 2132-2135.
[3] Y. K. Sun, S. M. Oh, H. K. Park, B. Scrosati, *Adv. Mater.*,**2011**, 23, 5050-5054.
[4] P. G. Bruce, B. Scrosati, J. M. Tarascon, *Angew. Chem. Int. Ed. Engl.,* **2008**, 47, 2930-2946.
[5] Y. Zhang, Q.-y. Huo, P.-p. Du, L.-z. Wang, A.-q. Zhang, Y.-h. Song, Y. LvG.-y. Li, *Synthetic Met.,* **2012**, 162, 1315-1326.
[6] M. K. Devaraju, I. Honma, *Adv. Energy Mater.,* **2012**, 2, 284-297.
[7] H. Wang, Y. Yang, Y. Liang, L. F. Cui, H. Sanchez Casalongue, Y. Li, G. Hong, Y. Cui, H. Dai, *Angew. Chem.,* **2011**, 123, 7502-7506.
[8] Z. Bakenov, I. Taniguchi, *J. Power Sources,* **2010**, 195, 7445-7451.
[9] D. Choi, D. Wang, I. T. Bae, J. Xiao, Z. Nie, W. Wang, V. V. Viswanathan, Y. J. Lee, J. G. Zhang, G. L. Graff, Z. Yang, J. Liu, *Nano. Lett.,* **2010**, 10, 2799-2805.
[10] L. Hu, B. Qiu, Y. Xia, Z. Qin, L. Qin, X. Zhou, Z. Liu, *J. Power Sources,* **2014**, 248, 246-252.
[11] S. K. Martha, J. Grinblat, O. Haik, E. Zinigrad, T. Drezen, J. H. Miners, I. Exnar, A. Kay, B. Markovsky, D. Aurbach, *Angew. Chem. Int. Ed. Engl.,* **2009**, 48, 8559-8563.
[12] N. S. Choi, Z. Chen, S. A. Freunberger, X. Ji, Y. K. Sun, K. Amine, G. Yushin, L. F. Nazar, J. Cho, P. G. Bruce, *Angew. Chem. Int. Ed. Engl.,* **2012**, 51, 9994-10024.
[13] Y. Wang, Y. Wang, E. Hosono, K. Wang, H. Zhou, *Angew. Chem. Int. Ed. Engl.,* **2008**, 47, 7461-7465.
[14] Y.-D. Cho, G. T.-K. Fey, H.-M. Kao, *J. Power Sources,* **2009**, 189, 256-262.
[15] G.-N. Zhu, C.-X. Wang, Y.-Y. Xia, *J. Electrochem. Soc.,* **2011**, 158, A102-A109.
[16] N. Liu, Z. Lu, J. Zhao, M. T. McDowell, H. W. Lee, W. Zhao, Y. Cui, *Nat. Nanotechnol.,* **2014**, 9, 187-192.
[17] N. Li, Q. Zhang, J. Liu, J. Joo, A. Lee, Y. Gan, Y. Yin, *Chem. Commun.,* **2013**, 49, 5135-5137.
[18] J. Liu, S. Z. Qiao, H. Liu, J. Chen, A. Orpe, D. Zhao, G. Q. Lu, *Angew. Chem. Int. Ed. Engl.,* **2011**, 50, 5947-5951.
[19] J. Liu, T. Yang, D. W. Wang, G. Q. Lu, D. Zhao, S. Z. Qiao, *Nat. Commun.,* **2013**, 4, 2798.
[20] A. B. Fuertes, P. Valle-Vigon, M. Sevilla, *Chem. Commun.,* **2012**, 48, 6124-6126.
[21] X. Fang, S. Liu, J. Zang, C. Xu, M. S. Zheng, Q. F. Dong, D. Sun, N. Zheng, *Nanoscale,* **2013**, 5, 6908-6916.
[22] Y. X. Chao Luo, Yujie Zhu, Yihang Liu, Shiyou Zheng, Ying Liu, Alex Langrock, Chunsheng Wang, *ACS Nano,* **2013**, 7, 8003-8010.
[23] A. H. Lu, G. P. Hao, Q. Sun, *Angew. Chem. Int. Ed. Engl.,* **2011**, 50, 9023-9025.
[24] J.-H. Jiang, L.-P. Zhu, X.-L. Li, Y.-Y. Xu, B.-K. Zhu, *J. Membrane Sci.,* **2010**, 364, 194-202.
[25] M. Yang, J. Ma, S. Ding, Z. Meng, J. Liu, T. Zhao, L. Mao, Y. Shi, X. Jin, Y. Lu, Z. Yang, *Macromol. Chem. Phys.,* **2006**, 207, 1633-1639.
[26] Z.-Y. Xi, Y.-Y. Xu, L.-P. Zhu, Y. Wang, B.-K. Zhu, *J. Membrane Sci.,* **2009**, 327, 244-253.

[27] B. Shareef, I. Waheed, K. Jalaot, *Orient. J. Chem.,* **2013**, 29, 1391-1397.
[28] W. Li, D. Chen, Z. Li, Y. Shi, Y. Wan, G. Wang, Z. Jiang, D. Zhao, *Carbon,* **2007**, 45, 1757-1763.
[29] C. Y. Wu, G. S. Cao, H. M. Yu, J. Xie, X. B. Zhao, *J. Phys. Chem. C,* **2011**, 115, 23090-23095.
[30] X. Zhang, Z. Xing, L. Wang, Y. Zhu, Q. Li, J. Liang, Y. Yu, T. Huang, K. Tang, Y. Qian, X. Shen, *J. Mater. Chem.,* **2012**, 22, 17864-17869.
[31] R. Dominko, M. Bele, M. Gaberscek, M. Remskar, D. Hanzel, S. Pejovnik, J. Jamnik, *J. Electrochem. Soc.,* **2005**, 152, A607-A610.
[32] Z. Qin, X. Zhou, Y. Xia, C. Tang, Z. Liu, *J. Mater. Chem.,* **2012**, 22, 21144-21153.
[33] M. Koltypin, D. Aurbach, L. Nazar, B. Ellis, *Electrochem. Solid-State Lett.,* **2007**, 10, A40-A44.
[34] J. Wang, J. Yang, Y. Tang, R. Li, G. Liang, T.-K. Sham, X. Sun, *J. Mater. Chem. A,* **2013**, 1, 1579-1586.
[35] N. Iltchev, Y. Chen, S. Okada, J.-i. Yamaki, *J. Power Sources,* **2003**, 119-121, 749-754.
[36] A. Yamada, S. C. Chung, K. Hinokuma, *J. Electrochem. Soc.,* **2001**, 148, A224-A229.
[37] H. Li, H. Zhou, *Chem. Commun.,* **2012**, 48, 1201-1217.

The table of contents entry

Core-shell structures of polyanion-type cathode materials (typically $LiMn_{0.5}Fe_{0.5}PO_4$) with uniform and conformal carbon layers were achieved by means of in-situ resorcinol-formaldehyde polymerization followed by a graphitization process. Systematic control on the coating layer identified that a 3 nm carbon coating produces the best battery performance**.** The carbon shell can also contribute to inhibit the Fe dissolution and reduce the exothermic heat released during cycling.

Key words: Core-shell structure, lithium ion batteries, carbon coating, thickness control, cathode materials

Zi-Xiang Chi, Wei Zhang, Xu-Sheng Wang, Fu-Quan Cheng, Ji-Tao Chen, An-Min Cao* and Li-Jun Wan*

Accurate surface control of core-shell structured $LiMn_{0.5}Fe_{0.5}PO_4$@C for improved battery performance